Medium induced resolution enhancement for broadband imaging

# Medium induced resolution enhancement for broadband imaging

## Habib Ammari[1], Josselin Garnier[2], Julien de Rosny[3] and Knut Sølna[4]

[1] Department of Mathematics and Applications, Ecole Normale Supérieure, 45 rue d'Ulm, F-75005 Paris, France
[2] Laboratoire de Probabilités et Modèles Aléatoires & Laboratoire Jacques-Louis Lions, Université Paris Diderot, F-75205 Paris Cedex 13, France
[3] Institut Langevin, UMR 7587, ESPCI ParisTech and CNRS, 1 rue Jussieu, F-75238 Paris Cedex 05, France
[4] Department of Mathematics, University of California, 92697 Irvine CA 92697, USA

E-mail: habib.ammari@ens.fr, garnier@math.univ-paris-diderot.fr, julien.derosny@espci.fr and ksolna@math.uci.edu

## Abstract

A number of recent studies discuss the phenomenon of super resolution, that is, the fact that a target can be localized with higher resolution than half a wavelength as suggested by the classical diffraction limit. Here we discuss a special type of super resolution corresponding to a high contrast in wave speed at the location of respectively the point of observation and the one of the target. We quantify the resolution achieved in this case and discuss image stability. It turns out that the image is stable with respect to measurement noise but very sensitive to medium uncertainty. The signal-to-noise ratio can in fact be significantly enhanced by exploiting resonance frequencies and we discuss this in detail, considering source as well as reflector broadband imaging.

Keywords: super-resolution, measurement noise, medium uncertainty

(Some figures may appear in colour only in the online journal)

## 1. Introduction

Time reversal of waves has been extensively studied in the last twenty years [6, 9–12]. A time-reversal mirror consists in a set of transducers that can be used as receivers or as transmitters. A classical time-reversal experiment consists of two steps. In the first step, a source generates a wave that propagates through a medium and is recorded by the time-

reversal mirror used as a set of receivers. In the second step, the time-reversal mirror is used as an array of transmitters, it re-emits the time-reversed recorded signals. It turns out that the wave focuses back at the initial source position, as if the wave were being played backwards. The refocusing properties have been studied experimentally, numerically and theoretically. They are characterized by diffraction-limited focal spots, that is to say, the size of the time-reversed focal spot is half the source carrier wavelength when the original source is point-like and the time-reversal mirror surrounds the region of interest.

Enhanced refocusing is a remarkable property observed in many time-reversal experiments and it can follow from several mechanisms. First, the diffraction limit can be overcome if the source is replaced by its time-reversed image during the second step of the time-reversal experiment. This requires to use an active sink that absorbs the time-reversed wave precisely at the original source location and at the exact refocusing time [7]. Second it is possible to obtain subwavelength focusing when the initial source is in the near field of the time-reversal mirror and the propagating medium is homogeneous and isotropic [8]. Third, focusing beyond the diffraction limit with far-field time reversal is possible, provided the medium in the near field of the original source has a high effective index and can radiate in the far field spatial information of the near field of the source. For instance a random distribution of scatterers or small resonators placed in the vicinity of the source can achieve this goal and locally reduce the effective wavelength [1, 13, 16–18].

Here we would like to analyze this last mechanism in the context of imaging, that is, in the context where the object (source or reflector) to be imaged is imbedded in a high-index (low-velocity) region. In such a case, the physical size of the object is small compared to the homogeneous wavelength of the wave used to probe the medium, but large (or at least not negligible) compared to the local wavelength evaluated in the low-velocity region. However the work on time reversal cited above does not apply directly to imaging. Indeed, imaging is different from time reversal. Similarly to time reversal, imaging consists of two steps, data acquisition and data processing. But contrarily to time reversal, the data processing is numerical and is based on the resolution of the wave equation in a fictitious medium (given *a priori* or estimated itself). The data processing may consist of the minimization of the misfit between the measured data and synthetic data obtained with the numerical solver (least-squares imaging), or it may consist of backpropagation, adjoint or matched field processing, that can be seen as simplified versions of least-square imaging [2, 3, 6, 20]. Experimental subwavelength imaging has been achieved using high-contrast materials or arrays of resonators [4, 15, 19]. In this case, the robustness of the procedure with respect to measurement noise and with respect to medium uncertainty is in fact the key issue.

In this paper we consider a simple one-dimensional framework. Our first objective is to estimate the location of a source that is in a section of anomalous low velocity. The picture that we want to analyze in some detail is that this allows us to estimate the location of the source with high accuracy. When the wave exits a section of low velocity its spatial support will be expanded, conversely if it enters the section of low velocity it will be compressed. This is what gives an apparent super resolution phenomenon. If one considers two nearby sources in a section of low velocity then at an observation point outside the section one would observe two pulses of relatively long wavelength, moreover, one would be able to resolve the locations of the sources with an accuracy greater than that corresponding to the wavelength at the point of observation. We want to analyze this phenomenon in some detail and quantify the resolution enhancement, moreover, examine its robustness with respect to measurement noise and medium uncertainty. Via our rigorous analysis we find that exploiting resonance frequencies is important in order to achieve enhancement of the signal-to-noise ratio.

Our second objective is to identify a reflector or inclusion in the section of low velocity with a source located outside of this section. We show that again the contrast in speed gives a resolution enhancement. We also set forth a detailed stability analysis incorporating both effects of medium uncertainty as well as measurement noise and again point to the importance of resonance frequencies.

In the analysis we shall use a mathematical framework similar to the one developed in [12]. However, here the focus is on a high contrast background medium rather than on highly oscillatory medium fluctuations.

The outline of the paper is as follows. We describe the medium and the acoustic propagation model in section 2 which articulates how the source is imbedded in a section of low velocity. Based on the recorded wave at a point outside the anomalous section we construct the image of the source point in section 3 with a focus on a discussion of resolution. In section 4 we show that the presence of measurement noise does not hamper resolution as long as a resolvability condition is satisfied, but that the imaging functions are very sensitive to medium uncertainty. In section 5 we generalize our discussion regarding source imaging to the case with reflector imaging. Finally, in section 6 we forward some concluding remarks.

## 2. Superresolution source imaging via medium contrast

### 2.1. Scalar wave model

We consider acoustic waves with conservation of momentum and mass for velocity $u(x, t)$ and pressure $p(x, t)$:

$$\rho_0 u_t + p_x = \delta(t)\delta(x - y)\sqrt{\zeta}, \tag{1}$$

$$c^{-2}p_t + \rho_0 u_x = 0, \tag{2}$$

for $\rho_0$ being the assumed constant density, $c$ the local velocity, and $\zeta = c\rho_0$ the impedance. Throughout the paper the subscripts stand for partial derivatives. An impulse source is imposed at the spatial location $y$. We assume dimensionless coordinates and a constant density so that we have

$$c^{-2}p_{tt} - p_{xx} = -\sqrt{\zeta}\,\delta(t)\delta'(x - y),$$

with $c$ being piecewise constant:

$$c(x) = \begin{cases} c_0/n & \text{if } x \in [-L/2, L/2] \\ c_0 & \text{otherwise} \end{cases}. \tag{3}$$

We assume that $n > 1$ and standard radiation conditions. We assume that the source is located in the section of low velocity: $y \in (-L/2, L/2)$. We shall also assume that we measure the wave at the location $y_o \in (L/2, \infty)$ and based on the recorded wave we aim to estimate the location of the source, that is $y$.

### 2.2. Wave decomposition

Below we follow the strategy developed in [12, chapter 3]. We expand first the wave field into right propagating modes ($A$) and left propagating modes ($B$) by the decomposition
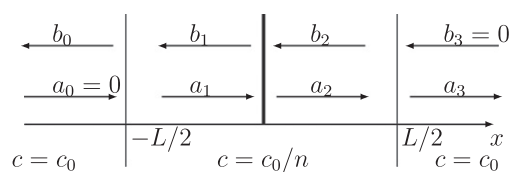
**Figure 1.** Wave amplitudes.

$$
\begin{bmatrix} A(x,t) \\ B(x,t) \end{bmatrix} = \begin{bmatrix} \dfrac{1}{\sqrt{\zeta(x)}} & \sqrt{\zeta(x)} \\ -\dfrac{1}{\sqrt{\zeta(x)}} & \sqrt{\zeta(x)} \end{bmatrix} \begin{bmatrix} p(x,t) \\ u(x,t) \end{bmatrix}, \tag{4}
$$

and thus

$$
\begin{bmatrix} p(x,t) \\ u(x,t) \end{bmatrix} = \frac{1}{2} \begin{bmatrix} \sqrt{\zeta(x)} & -\sqrt{\zeta(x)} \\ \dfrac{1}{\sqrt{\zeta(x)}} & \dfrac{1}{\sqrt{\zeta(x)}} \end{bmatrix} \begin{bmatrix} A(x,t) \\ B(x,t) \end{bmatrix}. \tag{5}
$$

Let the Fourier transforms be defined by

$$
\hat{A}(x,\omega) = \int A(x,t) e^{i\omega t} dt, \quad \hat{B}(x,\omega) = \int B(x,t) e^{i\omega t} dt,
$$

then we have from (1), (2):

$$
\hat{A}_x - \frac{i\omega}{c(x)} \hat{A} = \delta(x-y), \quad \hat{B}_x + \frac{i\omega}{c(x)} \hat{B} = -\delta(x-y), \tag{6}
$$

for $x \neq \pm L/2$. We introduce the complex amplitudes $a$ and $b$ of the propagating waves

$$
\hat{A}(x,\omega) = a(x,\omega) e^{i\omega\tau(x)}, \quad \hat{B}(x,\omega) = b(x,\omega) e^{-i\omega\tau(x)}, \tag{7}
$$

with the travel time defined by

$$
\tau(x) = \int_0^x \frac{dx'}{c(x')} = \begin{cases} -\dfrac{nL}{2c_0} + \dfrac{x+L/2}{c_0} & \text{for } x < -L/2 \\[2mm] \dfrac{nx}{c_0} & \text{for } -L/2 < x < L/2. \\[2mm] \dfrac{nL}{2c_0} + \dfrac{x-L/2}{c_0} & \text{for } L/2 < x \end{cases}
$$

The travel time is defined with respect to the origin but any other point could have been used. From (6) and (7) the amplitudes $a$, $b$ are piecewise constant over the intervals where there is no source and no jump in the medium parameter:

$$
a(x,\omega) = \begin{cases} a_0(\omega) & \text{for } x < -L/2 \\ a_1(\omega) & \text{for } -L/2 < x < y \\ a_2(\omega) & \text{for } y < x < L/2 \\ a_3(\omega) & \text{for } L/2 < x \end{cases},
$$

and similarly for $b(x,\omega)$, see figure 1.

**Interface conditions.** At the interface $x = L/2$, the local speed of sound $c$ and the local impedance $\zeta$ jump, so the continuity of $\hat{p}$ and $\hat{u}$:

$$\begin{bmatrix} \hat{p} \\ \hat{u} \end{bmatrix} \left( (L/2)^+ \right) = \begin{bmatrix} \hat{p} \\ \hat{u} \end{bmatrix} \left( (L/2)^- \right)$$

gives jump conditions for the amplitudes of the left and right propagating modes in view of (5):

$$\begin{bmatrix} \sqrt{\zeta} & -\sqrt{\zeta} \\ \frac{1}{\sqrt{\zeta}} & \frac{1}{\sqrt{\zeta}} \end{bmatrix} \begin{bmatrix} \hat{A} \\ \hat{B} \end{bmatrix} \left( (L/2)^+ \right) = \begin{bmatrix} \sqrt{\zeta} & -\sqrt{\zeta} \\ \frac{1}{\sqrt{\zeta}} & \frac{1}{\sqrt{\zeta}} \end{bmatrix} \begin{bmatrix} \hat{A} \\ \hat{B} \end{bmatrix} \left( (L/2)^- \right), \tag{8}$$

and similarly at the interface $x = -L/2$. If we introduce the interface coefficients $r^\pm$ and the jump matrices $\mathbf{J}^\pm$:

$$r^\pm = \frac{1}{2}\left( \frac{1}{\sqrt{n}} \pm \sqrt{n} \right), \quad \mathbf{J}^\pm = \begin{bmatrix} r^+ & \pm r^- \\ \pm r^- & r^+ \end{bmatrix},$$

then (8) reads

$$\begin{bmatrix} \hat{A} \\ \hat{B} \end{bmatrix} \left( (L/2)^+ \right) = \mathbf{J}^- \begin{bmatrix} \hat{A} \\ \hat{B} \end{bmatrix} \left( (L/2)^- \right),$$

and similary

$$\begin{bmatrix} \hat{A} \\ \hat{B} \end{bmatrix} \left( (-L/2)^+ \right) = \mathbf{J}^+ \begin{bmatrix} \hat{A} \\ \hat{B} \end{bmatrix} \left( (-L/2)^- \right).$$

Therefore

$$\begin{bmatrix} a_3(\omega)\mathrm{e}^{i\frac{\omega n L}{2c_0}} \\ b_3(\omega)\mathrm{e}^{-i\frac{\omega n L}{2c_0}} \end{bmatrix} = \mathbf{J}^- \begin{bmatrix} a_2(\omega)\mathrm{e}^{i\frac{\omega n L}{2c_0}} \\ b_2(\omega)\mathrm{e}^{-i\frac{\omega n L}{2c_0}} \end{bmatrix},$$

$$\begin{bmatrix} a_1(\omega)\mathrm{e}^{-i\frac{\omega n L}{2c_0}} \\ b_1(\omega)\mathrm{e}^{i\frac{\omega n L}{2c_0}} \end{bmatrix} = \mathbf{J}^+ \begin{bmatrix} a_0(\omega)\mathrm{e}^{-i\frac{\omega n L}{2c_0}} \\ b_0(\omega)\mathrm{e}^{i\frac{\omega n L}{2c_0}} \end{bmatrix}. \tag{9}$$

**Radiation conditions.** The radiation condition gives that

$$b_3(\omega) = 0, \qquad a_0(\omega) = 0, \tag{10}$$

that is, no energy is coming in from $\pm\infty$.

**Source conditions.** Integrating (6) accross the source location $y$ we get the jump relations $[\hat{A}]_{y^-}^{y^+} = 1$ and $[\hat{B}]_{y^-}^{y^+} = -1$, and therefore

$$a_2(\omega) = a_1(\omega) + \mathrm{e}^{-i\frac{\omega n y}{c_0}}, \tag{11}$$

$$b_2(\omega) = b_1(\omega) - \mathrm{e}^{i\frac{\omega n y}{c_0}}. \tag{12}$$

The relations (9), (10), (11), and (12) now give eight equations for the eight unknowns $a_j$, $b_j$, $j = 0, \ldots, 3$. We assume that we observe the transmitted wave at $y_o > L/2$ within the frequency band of the measurement device, that is we measure $a_3(\omega)\mathrm{e}^{i\omega\tau(y_o)}$ for $\omega \in [\omega_c - \Omega/2, \omega_c + \Omega/2]$, where $\omega_c$ is the central (angular) frequency and $\Omega$ is the bandwidth, with $\Omega < 2\omega_c$. We next identify the explicit expression for the observation.

### 2.3. Wave recordings

We have available the frequency response:

$$\left\{ a_{\mathrm{mes}}(\omega),\, \omega \in \left[ \omega_c - \Omega/2,\, \omega_c + \Omega/2 \right] \right\},$$

where $a_{\mathrm{mes}}(\omega)$ is the measured complex amplitude $a_3(\omega)e^{i\omega\tau(y_o)}$ of the wave recorded at $y_o$ from which a known phase is removed:

$$a_{\mathrm{mes}}(\omega) = a_3(\omega)e^{i\omega\tau(y_o)}e^{-i\frac{\omega}{c_0}\frac{nL}{2} - i\frac{\omega}{c_0}\left(y_o - \frac{L}{2}\right)}. \tag{13}$$

The phase $\frac{\omega}{c_0}\frac{nL}{2} + \frac{\omega}{c_0}(y_o - \frac{L}{2})$ is known provided $n$ is known and then it compensates exactly for $\omega\tau(y_o)$.

We introduce the reflection and transmission coefficients associated with the interface at $L/2$:

$$\mathcal{R} = -\frac{r^-}{r^+} = \frac{n-1}{n+1}, \quad \mathcal{T} = \frac{1}{r^+} = \frac{2\sqrt{n}}{1+n}. \tag{14}$$

Note that $\mathcal{T}^2 + \mathcal{R}^2 = 1$ and that the reflection coefficient is close to 1 when $n \gg 1$ and it can be expanded as $\mathcal{R} = 1 - 2/n + O(1/n^2)$.

From (9), (10), (11), and (12), the observed amplitude can be expressed as:

$$a_{\mathrm{mes}}(\omega) = \mathcal{T}e^{-i\frac{\omega ny}{c_0}}\frac{1 - \mathcal{R}e^{2i\frac{\omega n(y+L/2)}{c_0}}}{1 - \mathcal{R}^2 e^{2i\frac{\omega nL}{c_0}}}. \tag{15}$$

It can be expanded as:

$$a_{\mathrm{mes}}(\omega) = \mathcal{T}e^{-i\frac{\omega ny}{c_0}}\sum_{j=0}^{\infty}\left(\mathcal{R}^2 e^{2i\frac{\omega nL}{c_0}}\right)^j - \mathcal{T}\mathcal{R}\,e^{i\frac{\omega n(y+L)}{c_0}}\sum_{j=0}^{\infty}\left(\mathcal{R}^2 e^{2i\frac{\omega nL}{c_0}}\right)^j,$$

with the first term ($j = 0$) in the first sum corresponding to the contribution of the right-going wave generated by the source in (11) that is directly transmitted through the interface. The other terms in this sum correspond to the contributions of the wave components that have been reflected back and forth in the section several times before being emitted out of the section, thus associated with a phase delay corresponding to the travel time back and forth through the section. The terms of the second sum correspond to the contributions of the left-going wave emitted by the source in (12).

## 3. Imaging functions

### 3.1. Matched field processing

The adjoint imaging function (or coherent matched field imaging function, inspired by the known properties of time reversal refocusing) is defined by [6, 20]:

$$\mathcal{I}_a(\hat{y}) = \frac{1}{2\Omega}\int_{\omega_c - \Omega/2}^{\omega_c + \Omega/2} a_{\mathrm{mes}}(\omega)\overline{\hat{a}(\hat{y}, \omega)}\,\mathrm{d}\omega + \mathrm{c.\,c.}, \tag{16}$$

where c.c. stands for 'complex conjugate' and the synthetic data $\hat{a}(\hat{y}, \omega)$ is defined as (15) but with the search point $\hat{y}$ instead of $y$:

$$\hat{a}\left(\hat{y},\,\omega\right) = \mathcal{T}e^{-i\frac{\omega n \hat{y}}{c_0}}\frac{1 - \mathcal{R}e^{2i\frac{\omega n\left(\hat{y}+L/2\right)}{c_0}}}{1 - \mathcal{R}^2 e^{2i\frac{\omega n L}{c_0}}}. \tag{17}$$

**Proposition 3.1.** *When* $\Omega \gg \frac{\pi c_0}{nL}$, *we have*

$$\mathcal{I}_a\left(\hat{y}\right) = \mathrm{sinc}\left(\frac{\Omega n\left(y - \hat{y}\right)}{2c_0}\right)\cos\left(\frac{\omega_c n\left(y - \hat{y}\right)}{c_0}\right)$$

$$- \frac{2\mathcal{R}}{1 + \mathcal{R}^2}\mathrm{sinc}\left(\frac{\Omega n\left(y + \hat{y} + L\right)}{2c_0}\right)\cos\left(\frac{\omega_c n\left(y + \hat{y} + L\right)}{c_0}\right), \tag{18}$$

*where sinc is the function* $\mathrm{sinc}(s) = \sin(s)/s$.

If $y,\,\hat{y} \in (-L/2,\,L/2)$ and are far away from $-L/2$ (that is farther than $l$ defined just below in (19)), then the second term in (18) can be neglected. This shows that the imaging function is a rapidly modulated function with a sinc envelope, and the width of the envelop (i.e. the resolution) is

$$l = \frac{\lambda_B}{n}, \tag{19}$$

where $\lambda_B$ is the wavelength associated with the bandwidth

$$\lambda_B = \frac{2\pi c_0}{\Omega}. \tag{20}$$

We stress that $\lambda_B$ is the wavelength associated to the bandwidth $\Omega$ at the observation point, while $l$ is the wavelength when evaluated at the location of the source, the slow medium section.

**Proof.** Substituting (17) into (16) we find that $\mathcal{I}_a$ is the sum of four terms. They can be addressed in the same way so we only compute the first of them:

$$\mathcal{I}_1\left(\hat{y}\right) = \frac{1}{\Omega}\int_{\omega_c - \Omega/2}^{\omega_c + \Omega/2}\frac{\mathcal{T}^2\cos\left(\frac{\omega n\left(\hat{y} - y\right)}{c_0}\right)}{\left|1 - \mathcal{R}^2 e^{2i\frac{\omega n L}{c_0}}\right|^2}\mathrm{d}\omega.$$

When $\Omega \gg \frac{\pi c_0}{nL}$, the denominator in the integrand is a rapidly-varying periodic function in $\omega$ that is bounded from below by the positive constant $(1 - \mathcal{R}^2)^2$. Therefore the periodic averaging theorem [14, chapter 4] gives

$$\mathcal{I}_1\left(\hat{y}\right) = \frac{\mathcal{T}^2}{\Omega}\left\langle\frac{1}{1 + \mathcal{R}^4 - 2\mathcal{R}^2\cos\left(\cdot\right)}\right\rangle\int_{\omega_c - \Omega/2}^{\omega_c + \Omega/2}\cos\left(\frac{\omega n\left(\hat{y} - y\right)}{c_0}\right)\mathrm{d}\omega,$$

where $\langle\cdot\rangle$ stands for an averaging over the periodic component. Since the value of the average is $1/(1 - \mathcal{R}^4)$ and $\mathcal{T}^2 = 1 - \mathcal{R}^2$, we get

$$\mathcal{I}_1\left(\hat{y}\right) = \frac{1}{1 + \mathcal{R}^2}\mathrm{sinc}\left(\frac{\Omega n\left(y - \hat{y}\right)}{2c_0}\right)\cos\left(\frac{\omega_c n\left(y - \hat{y}\right)}{c_0}\right).$$

The calculations of the three other terms give the desired result.                    □

A conventional incoherent matched field imaging function is [6, 20]

$$\mathcal{I}_\mathrm{b}(\hat{y}) = \frac{1}{\Omega} \int_{\omega_c - \Omega/2}^{\omega_c + \Omega/2} \left| a_\mathrm{mes}(\omega) \overline{\hat{a}(\hat{y}, \omega)} \right|^2 \mathrm{d}\omega, \tag{21}$$

where the synthetic data $\hat{a}(\hat{y}, \omega)$ is defined by (17) (it is also known as incoherent broadband Bartlett processor [5]).

**Proposition 3.2.** *When* $\Omega \gg \frac{\pi c_0}{nL}$, *we have*

$$\mathcal{I}_\mathrm{b}(\hat{y}) = \frac{1 + \mathcal{R}^4}{\mathcal{T}^2 \left( 1 + \mathcal{R}^2 \right)^3} \left\{ \left( 1 + \mathcal{R}^2 \right)^2 + 2\mathcal{R}^2 \mathrm{sinc}\left( \frac{\Omega n \left( y - \hat{y} \right)}{c_0} \right) \cos\left( \frac{2\omega_c n \left( y - \hat{y} \right)}{c_0} \right) \right.$$

$$\left. + 2\mathcal{R}^2 \mathrm{sinc}\left( \frac{\Omega n \left( y + \hat{y} + L \right)}{c_0} \right) \cos\left( \frac{2\omega_c n \left( y + \hat{y} + L \right)}{c_0} \right) \right\}$$

$$\frac{2\mathcal{R}\left( 1 + \mathcal{R}^4 \right)}{\mathcal{T}^2 \left( 1 + \mathcal{R}^2 \right)^2} \left\{ \mathrm{sinc}\left( \frac{\Omega n \left( 2y + L \right)}{2c_0} \right) \cos\left( \frac{\omega_c n \left( 2y + L \right)}{c_0} \right) \right.$$

$$\left. + \mathrm{sinc}\left( \frac{\Omega n \left( 2\hat{y} + L \right)}{2c_0} \right) \cos\left( \frac{\omega_c n \left( 2\hat{y} + L \right)}{c_0} \right) \right\}. \tag{22}$$

Here the last three terms vanish if $y$ and $\hat{y}$ are far enough from $-L/2$ or $L/2$ (that is farther than $l$ in (19)). This incoherent imaging function has approximately the same resolution properties as the coherent imaging imaging function $\mathcal{I}_\mathrm{a}$, it has in fact better resolution by a factor two. However it possesses a large background contrarily to $\mathcal{I}_\mathrm{a}$. This is quite problematic in particular when there are several sources, as the overlap and interaction of the backgrounds and peaks become complicated, while $\mathcal{I}_\mathrm{a}$ presents the sum of the peaks by linearity of this imaging function. This justifies the fact that we will focus our attention to $\mathcal{I}_\mathrm{a}$ and its variants in the following.

**Proof.** The calculations follow the same lines as in the proof of proposition 3.1. When $\Omega \gg \frac{\pi c_0}{nL}$, the periodic averaging theorem gives

$$\mathcal{I}_\mathrm{b}(\hat{y}) = \frac{\mathcal{T}^4}{\Omega} \left\langle \frac{1}{\left( 1 + \mathcal{R}^4 - 2\mathcal{R}^2 \cos(\cdot) \right)^2} \right\rangle \int_{\omega_c - \Omega/2}^{\omega_c + \Omega/2} \left( 1 + \mathcal{R}^2 \right)^2$$

$$+ 2\mathcal{R}^2 \cos\left( \frac{2\omega n \left( \hat{y} - y \right)}{c_0} \right) + 2\mathcal{R}^2 \cos\left( \frac{2\omega n \left( \hat{y} + y + L \right)}{c_0} \right)$$

$$- 2\mathcal{R}\left( 1 + \mathcal{R}^2 \right) \left( \cos\left( \frac{\omega n \left( 2y + L \right)}{c_0} \right) + \cos\left( \frac{\omega n \left( 2\hat{y} + L \right)}{c_0} \right) \right) \mathrm{d}\omega,$$

where $\langle \cdot \rangle$ stands for an averaging over the periodic component. Since the value of the average is $(1 + \mathcal{R}^4)/(1 - \mathcal{R}^4)^3$ and $\mathcal{T}^2 = 1 - \mathcal{R}^2$, we get the desired result. $\qquad\square$
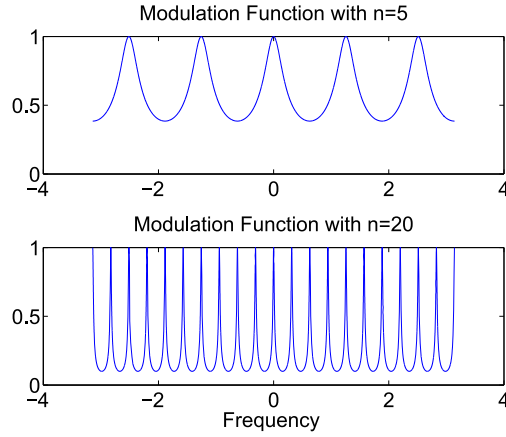
**Figure 2.** The modulation function $|(1 - \mathcal{R}^2)/(1 - \mathcal{R}^2 e^{iun})|$ as function of dimensionless frequency $u$ for $n = 5, 20$.

### 3.2. Simplified adjoint imaging

In figure 2 we plot the modulation function

$$
\left| \frac{1 - \mathcal{R}^2}{1 - \mathcal{R}^2 e^{2i\frac{\omega nL}{c_0}}} \right|
$$

for $n = 5$ and for $n = 20$ as function of the dimensionless frequency $2\omega L/c_0$. Note the singular behavior in $n$. It means that, for large $n$, the adjoint imaging function only uses the observations at the set of discrete frequencies where this factor is unity. This motivates the introduction of a simplified version of the adjoint imaging function

$$
\mathcal{I}_\mathrm{p}(\hat{y}) = \frac{\Delta\omega}{2\Omega} \sum_{m=-\infty}^{\infty} I_{(\omega_c - \Omega/2, \omega_c + \Omega/2)} \left( |\omega_m| \right) a_\mathrm{mes}(\omega_m) \overline{\hat{a}(\hat{y}, \omega_m)}, \tag{23}
$$

where $I_B$ is the indicator function on $B$ and

$$
\omega_m = m\Delta\omega, \qquad \Delta\omega = \frac{\pi c_0}{nL} = \frac{2\pi}{\tau_L}, \tag{24}
$$

with $\tau_L$ being the two-way travel time of the low-velocity section.

**Proposition 3.3.** *When $\Omega \gg \Delta\omega$ and $y$ is not within the distance $l$ (defined by (19)) of the boundaries $\pm L/2$, then we have*

$$
\mathcal{I}_\mathrm{p}(\hat{y}) = \frac{1 + \mathcal{R}^2}{\mathcal{T}^2} \mathrm{sinc}\left( \frac{\Omega n (y - \hat{y})}{2c_0} \right) \cos\left( \frac{\omega_c n (y - \hat{y})}{c_0} \right). \tag{25}
$$

The adjoint imaging function and simplified adjoint imaging function have the same resolution, but the simplified version has an enhanced amplitude when $n$ is large (since $(1 + \mathcal{R}^2)/\mathcal{T}^2 \simeq n/2$). This comes from the fact that the simplified version focuses on the important contributions of the measured data at the resonant frequencies.
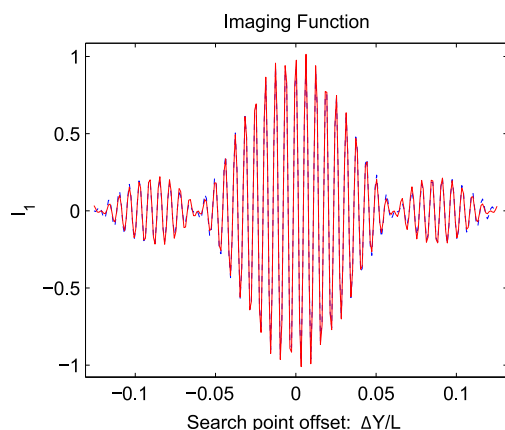
**Figure 3.** Theoretical imaging function $\mathcal{I}_\mathrm{p}$ given by (25) and normalized to one (blue dashed line) for $\Omega n L/c_0 = 100$ and $\omega_c/\Omega = 10$ as function of relative offset $\Delta y/L = (y - \hat{y})/L$. Imaging function defined by (23) and normalized to one (red solid line) for $n = 5$ and $y = 0$.

**Proof.** The expression of $\hat{a}$ becomes simpler when evaluated at the resonant frequencies:

$$\hat{a}(\hat{y}, \omega_m) = \frac{1}{\mathcal{T}} e^{-i\frac{\omega_m n \hat{y}}{c_0}} \left( 1 - (-1)^m \mathcal{R} e^{2i\frac{\omega_m n \hat{y}}{c_0}} \right),$$

where we have used the fact that $\exp(i\omega_m n L/c_0) = (-1)^m$. Since

$$a_\mathrm{mes}(\omega_m) = \frac{1}{\mathcal{T}} e^{-i\frac{\omega_m n y}{c_0}} \left( 1 - (-1)^m \mathcal{R} e^{2i\frac{\omega_m n y}{c_0}} \right),$$

the imaging function has the form

$$\mathcal{I}_\mathrm{p}(\hat{y}) = \frac{\Delta\omega}{2\Omega} \sum_{m=-\infty}^{\infty} I_{(\omega_c-\Omega/2,\omega_c+\Omega/2)}\left(\left|\omega_m\right|\right) \hat{a}(y, \omega_m) \overline{\hat{a}(\hat{y}, \omega_m)},$$

and it has several contributions:

$$
\begin{aligned}
\mathcal{I}_\mathrm{p}(\hat{y}) = {} & \frac{\Delta\omega\left(1 + \mathcal{R}^2\right)}{2\Omega\mathcal{T}^2} \sum_{m=-\infty}^{\infty} I_{(\omega_c-\Omega/2,\omega_c+\Omega/2)}\left(\left|\omega_m\right|\right) \cos\left(\frac{\omega_m n(\hat{y}-y)}{c_0}\right) \\
& - \frac{\Delta\omega\mathcal{R}}{\Omega\mathcal{T}^2} \sum_{m'=-\infty}^{\infty} I_{(\omega_c-\Omega/2,\omega_c+\Omega/2)}\left(\left|\omega_{2m'}\right|\right) \cos\left(\frac{\omega_{2m'} n(\hat{y}+y)}{c_0}\right) \\
& + \frac{\Delta\omega\mathcal{R}}{\Omega\mathcal{T}^2} \sum_{m'=-\infty}^{\infty} I_{(\omega_c-\Omega/2,\omega_c+\Omega/2)}\left(\left|\omega_{2m'+1}\right|\right) \cos\left(\frac{\omega_{2m'+1} n(\hat{y}+y)}{c_0}\right),
\end{aligned}
$$

where the signs of the terms derive from the factors $(-1)^m$. If $\Delta\omega \ll \Omega$ and $y$ is not within the distance $l$ (defined by (19)) of the boundaries $\pm L/2$, then we can use the continuum approximation for the sums, we find that the second and third sums cancel each other and that the first sum can be replaced by the expression (25).                                           $\square$

In figure 3 the blue dashed line is the theoretical imaging function (25) normalized to one plotted as function of relative offset $\Delta y/L = (y - \hat{y})/L$ for $\Omega n L/c_0 = 100$ and $\omega_c/\Omega = 10$.

The red solid line is the exact imaging function (23) (also normalized to one) in the case with $n = 5$ and $y = 0$ and is seen to almost coincide with the asymptotic form (25).

## 4. Stability and resolvability

We discuss in this section the robustness of the imaging function (23) with respect to additive measurement noise and medium uncertainty.

### 4.1. Robustness with respect to measurement noise

Assume that the measurements are corrupted by an additive noise so that we observe:

$$a_3(\omega) + \text{noise}$$

Then we have the generalization of (15)

$$a_{\text{mes}}(\omega) = e^{-i\frac{\omega ny}{c_0}} \left( 1 - \mathcal{R}e^{2i\frac{\omega n(y+L/2)}{c_0}} \right) \frac{\mathcal{T}}{1 - \mathcal{R}^2 e^{2i\frac{\omega nL}{c_0}}} + W(\omega),$$

where $W(\omega)$ models the measurement noise. The observations at the set of discrete frequencies $\omega_{\text{m}}$ are:

$$a_{\text{mes}}(\omega_m) = \frac{1}{\mathcal{T}} e^{-i\frac{\omega_m ny}{c_0}} \left( 1 - (-1)^m \mathcal{R}e^{2i\frac{\omega_m ny}{c_0}} \right) + \sigma w_m,$$

where $\sigma$ is the standard deviation of the measurement noise and $w_m$ is assumed to be an independent and identically distributed sequence of zero mean and unit variance complex circular random variables.

The expectation of the imaging function (23) is

$$\mathbb{E}\left[ \mathcal{I}_{\text{p}}(\hat{y}) \right] = \frac{\Delta\omega}{2\Omega} \sum_{m=-\infty}^{\infty} I_{(\omega_c - \Omega/2, \omega_c + \Omega/2)} \left( |\omega_m| \right) \hat{a}(y, \omega_m) \overline{\hat{a}(\hat{y}, \omega_m)}$$

and it is given by (25). The variance is given in the following proposition.

**Proposition 4.1.** *If $\Delta\omega \ll \Omega$, then*

$$Var\left[ \mathcal{I}_{\text{p}}(\hat{y}) \right] = \frac{\Delta\omega\sigma^2}{2\Omega} \frac{1 + \mathcal{R}^2}{\mathcal{T}^2}. \tag{26}$$

**Proof.** The fluctuations of the imaging function have the form

$$V(\hat{y}) = \mathcal{I}_{\text{p}}(\hat{y}) - \mathbb{E}\left[ \mathcal{I}_{\text{p}}(\hat{y}) \right]$$

$$= \frac{\Delta\omega\sigma}{2\Omega\mathcal{T}} \sum_{m=-\infty}^{\infty} I_{(\omega_c - \Omega/2, \omega_c + \Omega/2)} \left( |\omega_m| \right) w_m e^{i\frac{\omega_m n\hat{y}}{c_0}} \left( 1 - (-1)^m \mathcal{R}e^{-2i\frac{\omega_m n\hat{y}}{c_0}} \right).$$

Since the $w_m$'s are independent and identically distributed with mean zero and variance one, we have

$$Var\left[ \mathcal{I}_{\text{p}}(\hat{y}) \right] = \frac{(\Delta\omega)^2 \sigma^2}{4\Omega^2 \mathcal{T}^2} \sum_{m=-\infty}^{\infty} I_{(\omega_c - \Omega/2, \omega_c + \Omega/2)} \left( |\omega_m| \right) \left| 1 - (-1)^m \mathcal{R}e^{2i\frac{\omega_m n\hat{y}}{c_0}} \right|^2.$$

By expanding the square modulus we can split the variance into several contributions:

$$
\begin{aligned}
Var\left[\mathcal{I}_{\mathrm{p}}(\hat{y})\right] =\; & \frac{(\Delta\omega)^2\sigma^2}{4\Omega^2}\frac{1+\mathcal{R}^2}{\mathcal{T}^2}\sum_{m=-\infty}^{\infty} I_{(\omega_c-\Omega/2,\,\omega_c+\Omega/2)}\left(\left|\omega_m\right|\right) \\
& -\frac{(\Delta\omega)^2\sigma^2\mathcal{R}}{2\Omega^2\mathcal{T}^2}\sum_{m'=-\infty}^{\infty} I_{(\omega_c-\Omega/2,\,\omega_c+\Omega/2)}\left(\left|\omega_{2\,m'}\right|\right)\cos\left(\frac{\omega_{2\,m'}n\hat{y}}{c_0}\right) \\
& +\frac{(\Delta\omega)^2\sigma^2\mathcal{R}}{2\Omega^2\mathcal{T}^2}\sum_{m'=-\infty}^{\infty} I_{(\omega_c-\Omega/2,\,\omega_c+\Omega/2)}\left(\left|\omega_{2\,m'+1}\right|\right)\cos\left(\frac{\omega_{2\,m'+1}n\hat{y}}{c_0}\right).
\end{aligned}
$$

In the case that $\Delta\omega \ll \Omega$, the second and third sums cancel each other and we get the desired result.                                                                                                     $\square$

As a result we find the signal-to-noise ratio (with $\mathcal{R} \simeq 1$ and $\mathcal{T} \simeq 2/\sqrt{n}$):

$$
\mathrm{SNR} = \frac{\mathbb{E}\left[\mathcal{I}_{\mathrm{p}}(y)\right]}{Var\left[\mathcal{I}_{\mathrm{p}}(\hat{y})\right]^{1/2}} \simeq \sqrt{\frac{n\Omega}{\Delta\omega\sigma^2}}. \tag{27}
$$

Note that the SNR increases with the number of periods in the modulation function (see figure 2) and also with $n$. This gives the following result.

**Corollary 4.2.** *In order to have a signal-to-noise ratio larger than unity for the imaging function $\mathcal{I}_{\mathrm{p}}$ defined by (23), we need*

$$
\sigma < \sqrt{\frac{n\Omega}{\Delta\omega}}. \tag{28}
$$

### 4.2. Robusteness with respect to medium uncertainty

In order to form the imaging function (23) we assumed a perfect knowledge of the medium, that is to say of the index of refraction $n$. In this subsection we assume that the underlying medium parameter $1/n$ is estimated with an error $\delta$: $1/\hat{n} = (1 + \delta)/n$. Then, denoting by $\hat{\omega}_m$ the estimated resonant frequencies:

$$
\widehat{\Delta\omega} = \frac{\pi c_0}{\hat{n}L} = \Delta\omega\,(1 + \delta), \qquad \hat{\omega}_m = m\widehat{\Delta\omega} = \omega_m\,(1 + \delta),
$$

and by $\hat{\mathcal{R}}$ and $\hat{\mathcal{T}}$ the estimated reflection and transmission coefficients (with $\hat{n}$ instead of $n$ in the formulas (14)), the imaging function (23) is defined by:

$$
\mathcal{I}_{\mathrm{p}}(\hat{y}) = \frac{\widehat{\Delta\omega}}{2\Omega}\sum_{m=-\infty}^{\infty} I_{(\omega_c-\Omega/2,\,\omega_c+\Omega/2)}\left(\left|\hat{\omega}_m\right|\right)a_{\mathrm{mes}}\left(\hat{\omega}_m\right)\frac{1}{\hat{\mathcal{T}}}\mathrm{e}^{i\frac{\omega_m n\hat{y}}{c_0}}\left(1 - (-1)^m\hat{\mathcal{R}}\mathrm{e}^{-2i\frac{\omega_m n\hat{y}}{c_0}}\right).
$$

Moreover, by (13), the phase removed in the measured amplitude $a_3(\omega)\mathrm{e}^{i\omega\tau(y_o)}$ is $\frac{\omega}{c_0}\frac{\hat{n}L}{2} + \frac{\omega}{c_0}(y_o - \frac{L}{2})$:
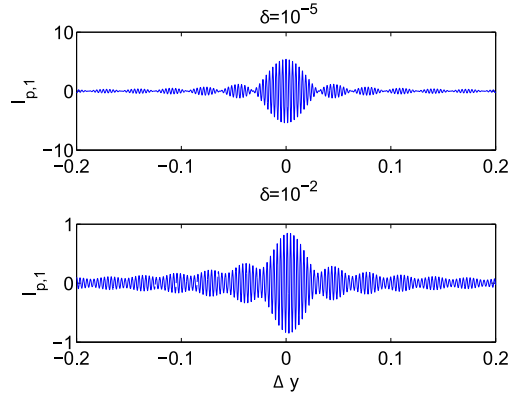
**Figure 4.** The imaging function $I_{p,1}$ as function of offset $\Delta y = \hat{y} - y(1 + \delta)$ for $\delta = 10^{-5}$ (top) and $10^{-2}$ (bottom) when $L = 1$, $n = 20$, $\Omega = 10$, $\omega_c = 100$, $c_0 = 1$ in the non-dimensionalized coordinates. This gives $(n\omega_c\tau_L)^{-1} = 1.25 \times 10^{-5}$ as a blurring threshold for $\delta$ and an optimal resolution corresponding to $l = 0.03$. Note that the blurring gives damping in imaging amplitude and lateral smearing.

$$a_{\mathrm{mes}}(\omega) = a_3(\omega)e^{i\omega\tau(y_o)}e^{-i\frac{\omega}{c_0}\frac{\hat{n}L}{2}-i\frac{\omega}{c_0}\left(y_o-\frac{L}{2}\right)},$$

which does not compensate exactly for $\omega\tau(y_o)$, so that it remains a phase error $\frac{\omega}{c_0(1+\delta)}\frac{nL}{2}\delta$.

**Proposition 4.3.** *The bias and blurring of the imaging function $\mathcal{I}_p$ defined by (23) are negligible if and only if*

$$\delta < \frac{1}{n\omega_c\tau_L}. \tag{29}$$

The condition (29) corresponds to an error in the estimate of the travel time $\tau_L$ that is smaller than $1/(n\omega_c)$ with $\omega_c$ being the carrier frequency of the source.

**Proof.** Recall that $\tau_L = 2nL/c_0$, and then the imaging function takes the form

$$\mathcal{I}_p(\hat{y}) = \frac{\widehat{\Delta\omega}}{2\Omega} \sum_{m=-\infty}^{\infty} I_{(\omega_c-\Omega/2,\omega_c+\Omega/2)}\left(|\hat{\omega}_m|\right) \frac{\mathcal{T}e^{i\omega_m\delta\frac{\tau_L}{4}}}{\hat{\mathcal{T}}\left(1 - \mathcal{R}^2e^{i\omega_m\delta\tau_L}\right)}$$

$$\times\left( e^{i\frac{\omega_m n\left(\hat{y}-y(1+\delta)\right)}{c_0}} - (-1)^m\mathcal{R}e^{i\frac{\omega_m n\left(\hat{y}+y(1+\delta)\right)}{c_0}}e^{i\omega_m\delta\frac{\tau_L}{2}}\right.$$

$$\left. -(-1)^m\hat{\mathcal{R}}\mathcal{R}e^{-i\frac{\omega_m n\left(\hat{y}+y(1+\delta)\right)}{c_0}} + \hat{\mathcal{R}}\mathcal{R}e^{i\frac{\omega_m n\left(y(1+\delta)-\hat{y}\right)}{c_0}}e^{i\omega_m\delta\frac{\tau_L}{2}}\right)$$

$$= \mathcal{I}_{p,1}(\hat{y}) + \mathcal{I}_{p,2}(\hat{y}) + \mathcal{I}_{p,3}(\hat{y}) + \mathcal{I}_{p,4}(\hat{y}).$$
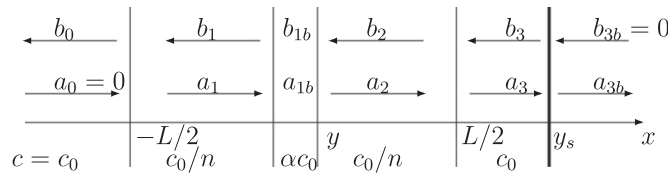
**Figure 5.** Wave amplitudes with a source at $y_s$ and a thin reflector at $[y - D, y]$.

We then get in particular

$$
\begin{aligned}
\mathcal{I}_{\mathrm{p},1}(\hat{y}) &= \frac{\widehat{\mathcal{T}\Delta\omega}}{2\hat{\mathcal{T}}\Omega} \sum_{m=-\infty}^{\infty} I_{(\omega_c-\Omega/2,\omega_c+\Omega/2)}\left(|\hat{\omega}_m|\right) \mathrm{e}^{i\omega_m\delta\frac{\tau_L}{4}} \sum_{j=0}^{\infty} \mathcal{R}^{2j}\mathrm{e}^{i\omega_m\left(\frac{n(\hat{y}-y(1+\delta))}{c_0}+j\delta\tau_L\right)} \\
&= \frac{\mathcal{T}}{\hat{\mathcal{T}}} \sum_{j=0}^{\infty} \mathcal{R}^{2j}\mathrm{sinc}\left(\frac{\Omega}{2}\left(\frac{n\Delta_{\hat{y}}}{c_0} + (j+1/4)\delta\tau_L\right)\right) \cos\left(\omega_c\left(\frac{n\Delta_{\hat{y}}}{c_0} + (j+1/4)\delta\tau_L\right)\right),
\end{aligned}
$$

with $\Delta_{\hat{y}} = \hat{y} - y(1 + \delta)$. Since $\mathcal{R} \simeq 1 - 2/n$ for large $n$, the support of the sum extends over $j$ of the order of $n$, and therefore there will be no blurring of the imaging function if and only if the term $\omega_c j\delta\tau_L$ does not blur the sum in $j$, that is to say, if (29) holds. Then the bias will also be small in the sense that $|y|\delta < \frac{\lambda_B}{4\pi n}$. $\qquad\square$

In figure 4 we show the imaging function for several values of the blurring parameter $\delta$. If $\delta > 1/(n\omega_c\tau_L)$ we indeed see that we get blurring in the form of smearing of the image and amplitude damping.

In conclusion the sensitivity to medium uncertainty increases with $n$. The results of this section show that the imaging function is stable with respect to measurement noise but unstable with respect to medium uncertainty.

## 5. Imaging of reflector

In this section we aim to image a reflector located at $y \in (-L/2, L/2)$ and with a source at $y_s \in (L/2, \infty)$. The medium is now modeled by

$$
c(x) = \begin{cases} c_0/n & \text{if } x \in [-L/2, y - D) \\ \alpha c_0 & \text{if } x \in [y - D, y] \\ c_0/n & \text{if } x \in (y, L/2] \\ c_0 & \text{otherwise} \end{cases}. \tag{30}
$$

The data are collected at the observation point $y_o \in (y_s, \infty)$ in the frequency band $[\omega_c - \Omega/2, \omega_c + \Omega/2]$, with $\Omega < 2\omega_c$.

### 5.1. Wave decomposition

The wave amplitudes are defined by (7) with $\tau(x) = \int_0^x 1/c(x')\mathrm{d}x'$. The right propagating mode amplitude is stepwise constant:

$$a(x, \omega) = \begin{cases} a_0(\omega) & \text{for } x < -L/2 \\ a_1(\omega) & \text{for } -L/2 < x < y - D \\ a_{1b}(\omega) & \text{for } y - D < x < y \\ a_2(\omega) & \text{for } y < x < L/2 \\ a_3(\omega) & \text{for } L/2 < x < y_s \\ a_{3b}(\omega) & \text{for } y_s < x \end{cases},$$

and similarly for the left propagating mode amplitude $b(x, \omega)$, see figure 5.

The coupling relations of the wave components at the boundary of the slow medium section are again given by (9). The analogues of the relations (10), (11), and (12) are now: (i) the radiation conditions

$$b_{3b}(\omega) = 0, \qquad a_0(\omega) = 0, \tag{31}$$

that is, no energy is coming in from $\pm\infty$, (ii) the source conditions

$$a_{3b}(\omega) = a_3(\omega) + e^{-i\omega\tau(y_s)}, \qquad b_{3b}(\omega) = b_3(\omega) - e^{i\omega\tau(y_s)}. \tag{32}$$

In addition we now have the interface reflection relations at $x = y - D$ and $x = y$:

$$\begin{bmatrix} a_{1b}(\omega)e^{i\omega\tau(y-D)} \\ b_{1b}(\omega)e^{-i\omega\tau(y-D)} \end{bmatrix} = \mathbf{J}_\alpha^- \begin{bmatrix} a_1(\omega)e^{i\omega\tau(y-D)} \\ b_1(\omega)e^{-i\omega\tau(y-D)} \end{bmatrix}, \tag{33}$$

$$\begin{bmatrix} a_2(\omega)e^{i\omega\tau(y)} \\ b_2(\omega)e^{-i\omega\tau(y)} \end{bmatrix} = \mathbf{J}_\alpha^+ \begin{bmatrix} a_{1b}(\omega)e^{i\omega\tau(y)} \\ b_{1b}(\omega)e^{-i\omega\tau(y)} \end{bmatrix}, \tag{34}$$

for

$$\mathbf{J}_\alpha^\pm = \begin{bmatrix} r_\alpha^+ & \pm r_\alpha^- \\ \pm r_\alpha^- & r_\alpha^+ \end{bmatrix}, \qquad r_\alpha^\pm = \frac{1}{2}\left( \frac{1}{\sqrt{\alpha n}} \pm \sqrt{\alpha n} \right). \tag{35}$$

This gives a total of 12 equations for the 12 unknowns.

We introduce the notation

$$\tau_1(y, D) = \tau(y - D) - \tau(-L/2) = n\frac{L/2 + y - D}{c_0}, \tag{36}$$

$$\tau_2(y, D) = \tau(y) - \tau(y - D) = \frac{D}{\alpha c_0}, \tag{37}$$

$$\tau_3(y, D) = \tau(L/2) - \tau(y) = n\frac{L/2 - y}{c_0}, \tag{38}$$

with the inclusion supported in $(y - D, y)$. Note first that the propagator matrix associated with the inclusion can be expressed by

$$\begin{bmatrix} a_2(\omega)e^{i\omega\tau(y)} \\ b_2(\omega)e^{-i\omega\tau(y)} \end{bmatrix} = \mathbf{J}_\alpha^+ \begin{bmatrix} e^{i\omega\tau_2(y,D)} & 0 \\ 0 & e^{-i\omega\tau_2(y,D)} \end{bmatrix} \mathbf{J}_\alpha^- \begin{bmatrix} a_1(\omega)e^{i\omega\tau(y-D)} \\ b_1(\omega)e^{-i\omega\tau(y-D)} \end{bmatrix}$$

$$= \begin{bmatrix} \overline{h_1(\omega, y, D)} & h_2(\omega, y, D) \\ \overline{h_2(\omega, y, D)} & h_1(\omega, y, D) \end{bmatrix} \begin{bmatrix} a_1(\omega)e^{i\omega\tau(y-D)} \\ b_1(\omega)e^{-i\omega\tau(y-D)} \end{bmatrix},$$

for

$$h_1(\omega, y, D) = \left(r_\alpha^+\right)^2 e^{-i\omega\tau_2(y,D)} - \left(r_\alpha^-\right)^2 e^{i\omega\tau_2(y,D)}, \tag{39}$$

$$h_2(\omega, y, D) = \left(r_\alpha^+ r_\alpha^-\right)\left(e^{-i\omega\tau_2(y,D)} - e^{i\omega\tau_2(y,D)}\right). \tag{40}$$

This gives the following expression for the amplitude of the reflection $a_{3b}(\omega)$ at an observation point $y_o \in (y_s, \infty)$:

$$a_{3b}(\omega) = e^{-i\omega\tau(y_s)} + e^{i\omega\left(\tau(y_s) - 2\tau(L/2)\right)}$$

$$\times \frac{c_2(\omega, y, D) - \mathcal{R}^2\overline{c_2(\omega, y, D)} - \mathcal{R}\left(c_1(\omega, y, D) - \overline{c_1(\omega, y, D)}\right)}{\overline{c_1(\omega, y, D)} - \mathcal{R}^2 c_1(\omega, y, D) - \mathcal{R}\left(\overline{c_2(\omega, y, D)} - c_2(\omega, y, D)\right)}, \tag{41}$$

for

$$c_1(\omega, y, D) = \left(e^{i\omega\tau_2(y,D)} - \mathcal{R}_\alpha^2 e^{-i\omega\tau_2(y,D)}\right) e^{i\omega\left(\tau_1(y,D) + \tau_3(y,D)\right)}, \tag{42}$$

$$c_2(\omega, y, D) = \mathcal{R}_\alpha\left(e^{i\omega\tau_2(y,D)} - e^{-i\omega\tau_2(y,D)}\right) e^{i\omega\left(-\tau_1(y,D) + \tau_3(y,D)\right)}, \tag{43}$$

where we have defined the reflection coefficient

$$\mathcal{R}_\alpha = -\frac{r_\alpha^-}{r_\alpha^+}. \tag{44}$$

## 5.2. Wave recordings

The observable quantity of interest is the complex amplitude $a_{3b}(\omega)e^{i\omega\tau(y_o)}$ observed at $y_o \in (y_s, \infty)$. We remove the original right-going wave and a known phase from this observable quantity to get

$$a_{\text{mes}}(\omega) = \left(a_{3b}(\omega)e^{i\omega\tau(y_o)} - e^{i\frac{\omega}{c_0}(y_o - y_s)}\right)e^{-i\frac{\omega}{c_0}\left(y_o + y_s - L\right)}. \tag{45}$$

Note that we have

$$\tau(y_o) - \tau(y_s) = \frac{1}{c_0}(y_o - y_s),$$

$$\tau(y_o) + \tau(y_s) - 2\tau(L/2) = \frac{1}{c_0}\left(y_o + y_s - L\right),$$

so that $a_{\text{mes}}(\omega)$ is of the form

$$a_{\text{mes}}(\omega) = \frac{c_2(\omega, y, D) - \mathcal{R}^2\overline{c_2(\omega, y, D)} - \mathcal{R}\left(c_1(\omega, y, D) - \overline{c_1(\omega, y, D)}\right)}{\overline{c_1(\omega, y, D)} - \mathcal{R}^2 c_1(\omega, y, D) - \mathcal{R}\left(\overline{c_2(\omega, y, D)} - c_2(\omega, y, D)\right)}. \tag{46}$$

When the inclusion is small such that $n\frac{\omega_c}{c_0}D \ll 1$, we have

$$a_{\text{mes}}(\omega) = d_0(\omega) + \frac{i\omega D}{c_0}d_1(\omega)$$

$$+ \frac{i\omega D}{c_0}d_2(\omega)\left(e^{-i\frac{\omega}{c_0}nL}e^{-2i\frac{\omega}{c_0}ny} + \mathcal{R}^2 e^{i\frac{\omega}{c_0}nL}e^{2i\frac{\omega}{c_0}ny}\right), \tag{47}$$

16

$$d_0(\omega) = \mathcal{R}\frac{1 - e^{2i\frac{\omega}{c_0}nL}}{1 - \mathcal{R}^2 e^{2i\frac{\omega}{c_0}nL}}$$

$$d_1(\omega) = \frac{2\mathcal{R}\left(1 - \mathcal{R}^2\right)e^{2i\frac{\omega}{c_0}nL}}{\left(1 - \mathcal{R}_\alpha^2\right)\left(1 - \mathcal{R}^2 e^{2i\frac{\omega}{c_0}nL}\right)^2}\left(n\left(1 - \mathcal{R}_\alpha^2\right) - \frac{1}{\alpha}\left(1 + \mathcal{R}_\alpha^2\right)\right), \quad (48)$$

$$d_2(\omega) = \frac{2\mathcal{R}_\alpha\left(1 - \mathcal{R}^2\right)e^{2i\frac{\omega}{c_0}nL}}{\left(1 - \mathcal{R}_\alpha^2\right)\alpha\left(1 - \mathcal{R}^2 e^{2i\frac{\omega}{c_0}nL}\right)^2}, \quad (49)$$

up to terms of smaller order $O(n^2\frac{\omega_c^2}{c_0^2}D^2)$, as shown in the appendix. Note that

- the leading-order term $d_0$ cancels at the set of discrete frequencies $\omega_m = m\Delta\omega$, $m = 1, 2, \ldots$, with $\Delta\omega$ defined by (24),
- the third term (proportional to $d_2$) in the expansion (47) contains the information about the inclusion location $y$.

When $D = 0$ we get

$$a_{\mathrm{mes}}(\omega) = \frac{\mathcal{R}\left(1 - e^{2i\frac{\omega}{c_0}nL}\right)}{1 - \mathcal{R}^2 e^{2i\frac{\omega}{c_0}nL}} = \mathcal{R} - \mathcal{T}^2\sum_{j=0}^{\infty}\mathcal{R}^{1+2j}e^{2i\frac{\omega}{c_0}nL(1+j)}, \quad (50)$$

corresponding to the direct reflection from the interface of the section at $L/2$ and then reflected signal components that have reverberated $j$ times in the section ($-L/2$, $L/2$). Note that the reflected signal is zero if the frequency $\omega$ is resonant (i.e. if the frequency is equal to $\omega_m = m\Delta\omega$ for some integer $m$). In this case the emitted wave probes in the most efficient way the section in ($-L/2$, $L/2$) as it is reflected back and forth coherently between the two interfaces and it does not come back to the right-half space $x > L/2$.

### 5.3. Imaging functions

Assume from now on that there is an inclusion. The adjoint imaging function is

$$\mathcal{I}_{\mathrm{ra}}\left(\hat{y}, \hat{D}\right) = \frac{1}{4\Omega}\int_{\omega_c - \Omega/2}^{\omega_c + \Omega/2}a_{\mathrm{mes}}(\omega)\overline{\hat{a}\left(\hat{y}, \hat{D}, \omega\right)}\mathrm{d}\omega + c.c., \quad (51)$$

where $\hat{a}(\hat{y}, \hat{D}, \omega)$ is given by (46) with $\hat{y}$ and $\hat{D}$ in place of $y$ and $D$. From the form (47) of $a_{\mathrm{mes}}$, we can see that the modulation functions $d_1$ and $d_2$ become highly concentrated at the set of discrete frequencies $\omega_{\mathrm{m}}$ defined by (24) for large $n$. This means that, for large $n$, the adjoint imaging function only uses the observations at the frequencies $\omega_{\mathrm{m}}$. As in the case of source imaging addressed in the previous section, this motivates the introduction of a simplified version of the adjoint imaging function:

$$\mathcal{I}_{\mathrm{ras}}\left(\hat{y}, \hat{D}\right) = \frac{\Delta\omega}{4\Omega}\sum_{m=-\infty}^{\infty}I_{(\omega_c - \Omega/2, \omega_c + \Omega/2)}\left(\left|\omega_m\right|\right)a_{\mathrm{mes}}(\omega_m)\overline{\hat{a}\left(\hat{y}, \hat{D}, \omega_m\right)}. \quad (52)$$

From the form (47) of $a_{\mathrm{mes}}$, we can see that, if we are only interested in the localization problem, then we should use

17

$$\mathcal{I}_{\mathrm{r1}}(\hat{y}) = \frac{\Delta\omega}{4\Omega} \sum_{m=-\infty}^{\infty} (-1)^m I_{(\omega_c - \Omega/2, \omega_c + \Omega/2)}\left(\left|\omega_m\right|\right)\left( -i\frac{\omega_m}{c_0} \right)$$

$$\times\left( e^{2i\frac{\omega_m}{c_0}n\hat{y}} + \mathcal{R}^2 e^{-2i\frac{\omega_m}{c_0}n\hat{y}} \right) a_{\mathrm{mes}}(\omega_m). \tag{53}$$

We analyze this imaging function in the following.

**First imaging function.** From the expression (50) in the absence of inclusion, it is appropriate to observe the field at the resonant frequencies $\omega_{\mathrm{m}}$ so that the recorded reflected wave associated to the inclusion is not buried in the reflected wave components asssociated to the boundaries of the section. In the presence of a small reflector with $n\frac{\omega_c}{c_0}D \ll 1$ we have

$$a_{\mathrm{mes}}(\omega_m) = \frac{\frac{2}{\alpha}(-1)^m \mathcal{R}_\alpha\left( e^{-2i\frac{\omega_m}{c_0}ny} + \mathcal{R}^2 e^{2i\frac{\omega_m}{c_0}ny} \right) + 2n\mathcal{R}\left( 1 - \mathcal{R}_\alpha^2 \right) - \frac{2}{\alpha}\mathcal{R}\left( 1 + \mathcal{R}_\alpha^2 \right)}{\left( 1 - \mathcal{R}_\alpha^2 \right)\left( 1 - \mathcal{R}^2 \right)}$$

$$\times i\frac{\omega_m D}{c_0}\left[ 1 + O\left( n\frac{\omega_c}{c_0}D \right) \right].$$

This is another (but analogous) motivation for the introduction of the imaging function (53).

When $\Omega$ is much larger than $\Delta\omega$, we can use the continuum approximation for the sums in (53) and we find that, unless the inclusion is close to $-L/2$ or $L/2$ within a distance of the order of $l$, the imaging function is given by

$$\mathcal{I}_{\mathrm{r1}}(\hat{y}) = \frac{2\mathcal{R}_\alpha}{\alpha\left( 1 - \mathcal{R}^2 \right)\left( 1 - \mathcal{R}_\alpha^2 \right)}\frac{\omega_c^2 D}{c_0^2}\left[ \frac{1 + \mathcal{R}^4}{2}\mathrm{sinc}\left( \frac{\Omega n(\hat{y} - y)}{c_0} \right)\cos\left( \frac{2\omega_c n(\hat{y} - y)}{c_0} \right) \right.$$

$$\left. + \mathcal{R}^2\mathrm{sinc}\left( \frac{\Omega n(\hat{y} + y)}{c_0} \right)\cos\left( \frac{2\omega_c n(\hat{y} + y)}{c_0} \right) \right], \tag{54}$$

for $\hat{y}$ far enough from $-L/2$ or $L/2$ (ie farther than $l$).

This imaging function can localize the inclusion with the resolution $l$ given by (19), but there is a ghost image: there are two peaks at $\hat{y} = \pm y$ and it is not easy to decide which of these two peaks corresponds to the position of the inclusion. Indeed the peak associated to the inclusion has an amplitude that is larger than the ghost peak, by a factor $(1 + \mathcal{R}^4)/(2\mathcal{R}^2)$, but this factor is close to one when $n \gg 1$.

When $n$ is large, the amplitude factor $2\mathcal{R}_\alpha/[\alpha(1 - \mathcal{R}^2)(1 - \mathcal{R}_\alpha^2)]$ in (54) is about $n^2/8$. This enhancement factor of the order of $n^2$ comes from the fact that the waves have been reflected back and forth about $n$ times within the section, and during each pass the interaction with the inclusion generates small scattered waves that build up coherently to generate the reflected signal. As a consequence this imaging function will be robust against measurement noise but sensitive to medium uncertainty (knowledge of $c_0/n$), as we will see in the next section.

**Second imaging function.** Another imaging function can be formed by using only the first arrivals of the recorded signals. Here we assume that $y - D > 0$, and that by a time windowing technique, we record only the components of the observable quantity $a_{3b}(\omega)e^{i\omega\tau(y_o)}$ that arrive before the time $(y_o + y_s - L + nL)/c_0$ at the observation point $y_o$. Note that the observable quantity $a_{3b}(\omega)e^{i\omega\tau(y_o)}$ is a sum of components of the form $e^{i\omega\tau}$ in the frequency domain (this can be seen by writing the denominator in (41) as a series expansion), or equivalently a sum of Dirac distributions $\delta(t - \tau)$ in the time domain. Therefore, the time windowing selects the components whose phases are of the form $e^{i\omega\tau}$ with

$\tau < (y_o + y_s - L + nL)/c_0$. After the time windowing we remove the original right-going wave $e^{i\omega(y_o - y_s)/c_0}$ and the known phase $\omega(y_o + y_s - L)/c_0$ as in (45), which gives the new data set $\tilde{a}_{\mathrm{mes}}(\omega)$. Compared to $a_{\mathrm{mes}}(\omega)$, the time windowing removes the components whose phases are of the form $e^{i\omega\tau}$ with $\tau > nL/c_0$. In particular, it removes the components of the recorded signals that arrive after the first echo from the boundary at $-L/2$. Indeed these components have phases of the form $e^{i\omega\tau}$ with $\tau \geqslant t_1 := 2(nL - (n - 1/\alpha)D)/c_0$, where $t_1$ is the time for a round trip from $L/2$ to $-L/2$, which is larger than $nL/c_0$ provided $D < L/2$.

By writing the denominator of $a_{\mathrm{mes}}(\omega)$ as a series expansion, we get an infinite sum with terms of the form $e^{i\omega\tau}$, and by keeping only those terms with $\tau \leqslant nL/c_0$, we find

$$\tilde{a}_{\mathrm{mes}}(\omega) = \mathcal{R} - \left(1 - \mathcal{R}^2\right) \sum_{j=1}^{J} \frac{2^j i^{-j} \mathcal{R}^{j-1} \mathcal{R}_\alpha^j \sin^j\left(\frac{\omega}{c_0}\frac{D}{\alpha}\right)}{\left(e^{-i\frac{\omega}{c_0}\frac{D}{\alpha}} - \mathcal{R}_\alpha^2 e^{i\frac{\omega}{c_0}\frac{D}{\alpha}}\right)^j} e^{i\frac{\omega}{c_0}nj(L-2y)},$$

where $J$ is the integer such that $(L - 2y)J < L \leqslant (L - 2y)(J + 1)$. The term $\mathcal{R}$ is the direct reflection from the interface at $L/2$. The first term ($j = 1$) of the sum is the wave that has been reflected by the inclusion and directly transmitted to the region $x > L/2$. The $j$th term of the sum is the wave that has been reflected by the inclusion and then reflected $j - 1$ times between the interface at $L/2$ and the inclusion before being transmitted to the region $x > L/2$. When $n\frac{\omega_c}{c_0}D \ll 1$ the new data can be expanded as

$$\tilde{a}_{\mathrm{mes}}(\omega) = \mathcal{R} + \frac{2i\omega D}{c_0} \frac{\mathcal{R}_\alpha\left(1 - \mathcal{R}^2\right)}{\alpha\left(1 - \mathcal{R}_\alpha^2\right)} e^{i\frac{\omega}{c_0}n(L-2y)}\left[1 + O\left(n\frac{\omega_c}{c_0}D\right)\right].$$

Additionally, if $n$ is large then the amplitude factor $[\mathcal{R}_\alpha(1 - \mathcal{R}^2)]/[\alpha(1 - \mathcal{R}_\alpha^2)]$ is approximately one. This gives the motivation for the following imaging function:

$$\mathcal{I}_{\mathrm{r2}}(\hat{y}) = \frac{1}{2\Omega} \int_{\omega_c - \Omega/2}^{\omega_c + \Omega/2} \left(-i\frac{\omega}{c_0}\right) e^{-i\frac{\omega}{c_0}n(L-2\hat{y})} \tilde{a}_{\mathrm{mes}}(\omega)\mathrm{d}\omega + \mathrm{c.c.} \qquad (55)$$

In the presence of a small reflector with $n\frac{\omega_c}{c_0}D \ll 1$ and with the inclusion farther than $l$ from the section boundaries it has the form

$$\mathcal{I}_{\mathrm{r2}}(\hat{y}) = \frac{2\mathcal{R}_\alpha\left(1 - \mathcal{R}^2\right)}{\alpha\left(1 - \mathcal{R}_\alpha^2\right)} \frac{\omega_c^2 D}{c_0^2} \mathrm{sinc}\left(\frac{\Omega n(\hat{y} - y)}{c_0}\right) \cos\left(\frac{2\omega_c n(\hat{y} - y)}{c_0}\right). \quad (56)$$

The resolution of this imaging function is $l$ given by (19) and there is no ghost in it contrarily to the imaging function (53). Note, however, that the amplitude is $n^2$ times smaller than the one of the previous imaging function (53), since the amplitude factor $[2\mathcal{R}_\alpha(1 - \mathcal{R}^2)]/[\alpha(1 - \mathcal{R}_\alpha^2)]$ is about 2 when $n$ is large. This is because we only exploit the first arrival in this imaging function, while the previous one exploited the full sequence of reflected waves. As a consequence this imaging function will be less robust with respect to measurement noise than the imaging function (53), but also less sensitive to medium uncertainty.

**Third imaging function.** In the previous section we obtained an image without a ghost as in the imaging function (53), however, at the expense of loosing a multiplicative factor of $n^2$ in the amplitude, which makes the imaging function sensitive to measurement noise. Moreover, this imaging function requires a time-windowing of the measured data. It is possible to get rid off the ghost in the imaging function (53) in a simpler way, at the expense of losing a multiplicative factor of the order of $n$ only. The idea is to add appropriate weights
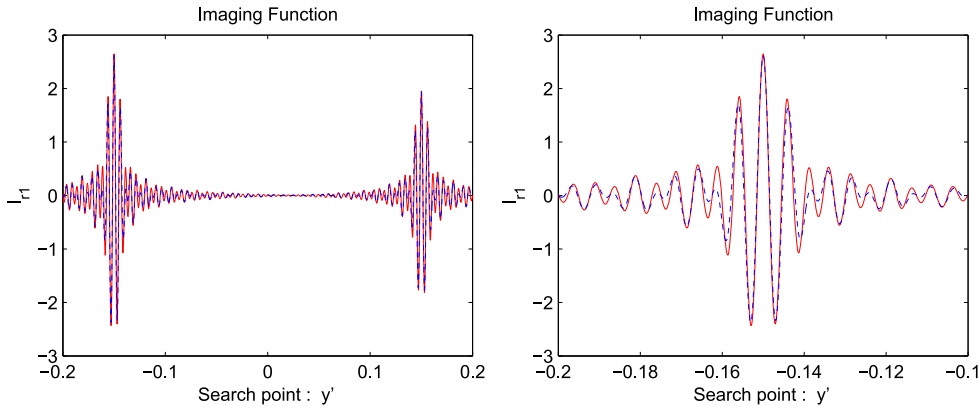
19

**Figure 6.** The imaging function $\mathcal{I}_{r1}(\hat{y})$ defined by (53) as function of search point $\hat{y}$ (red solid line) and its theoretical value (54) (blue dashed line). The right picture is a zoom of the left picture.

to the two terms in the imaging function (53) to cancel the ghost. Consider the imaging function

$$\mathcal{I}_{r3}(\hat{y}) = \frac{\Delta\omega}{4\Omega} \sum_{m=-\infty}^{\infty} (-1)^m I_{(\omega_c - \Omega/2, \omega_c + \Omega/2)}\left(\left|\omega_m\right|\right)\left(-i\frac{\omega_m}{c_0}\right)$$
$$\times \left(e^{2i\frac{\omega_m}{c_0}n\hat{y}} - \mathcal{R}^2 e^{-2i\frac{\omega_m}{c_0}n\hat{y}}\right) a_{\text{mes}}(\omega_m). \tag{57}$$

Here, the sign of the factor involving $\mathcal{R}^2$ is chosen to cancel the ghost term. When $\Omega$ is much larger than $\Delta\omega$, in the presence of a small reflector with $n\frac{\omega_c}{c_0}D \ll 1$ and with the inclusion farther than $l$ from the section boundaries, the imaging function is given by

$$\mathcal{I}_{r3}(\hat{y}) = \frac{\left(1 + \mathcal{R}^2\right)\mathcal{R}_\alpha}{\alpha\left(1 - \mathcal{R}_\alpha^2\right)} \frac{\omega_c^2 D}{c_0^2} \text{sinc}\left(\frac{\Omega n\left(\hat{y} - y\right)}{c_0}\right) \cos\left(\frac{2\omega_c n\left(\hat{y} - y\right)}{c_0}\right), \quad (58)$$

for $\hat{y}$ far enough from $-L/2$ or $L/2$.

This imaging function has the same resolution (19) as (53), it does not have any ghost image, and it is better than the imaging function (55) because it uses all the reflected waves and not only the first arrival. However, compared to (53), it has lost a multiplicative factor of the order of $n$. Indeed, when $n$ is large, the amplitude factor $(1 + \mathcal{R}^2)\mathcal{R}_\alpha/[\alpha(1 - \mathcal{R}_\alpha^2)]$ is about $n$. This shows that it has less robustness with respect to measurement noise than the imaging function (53), as we will see in the next section.

**Numerical illustrations.** We illustrate the performance of the imaging functions $\mathcal{I}_{r1}(\hat{y})$, $\mathcal{I}_{r2}(\hat{y})$, and $\mathcal{I}_{r3}(\hat{y})$ for some values of the parameters. We choose in a non-dimensionalized setting: $n = 5$; $\omega_c = 32\pi$; $\Omega = \omega_c/2$; $L = 10$; $D = 10^{-4}$; $\alpha = 1$; $c_0 = 1$, moreover the reflector is located at $y = -0.15$. This gives a resolution of $l = 0.025$.

In figure 6 we show the imaging function $\mathcal{I}_{r1}(\hat{y})$ defined by (53) with the red solid line and its theoretical value (54) by the dashed blue line.

In figure 7 we show the imaging function $\mathcal{I}_{r2}(\hat{y})$ defined by (55) with the red solid line and its theoretical value (56) by the dashed blue line.

In figure 8 we show the imaging function $\mathcal{I}_{r3}(\hat{y})$ defined by (57) with the red solid line and its theoretical value (58) by the dashed blue line. Note that the ghost is now suppressed,
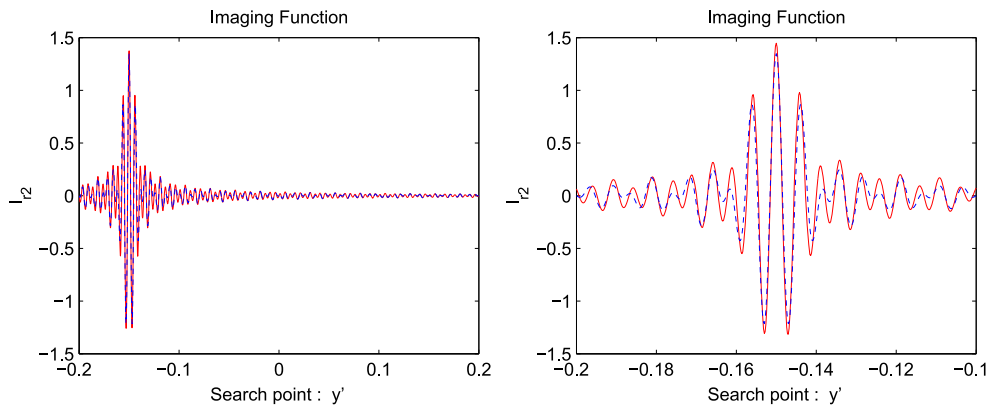
**Figure 7.** The imaging function $\mathcal{I}_{r2}(\hat{y})$ defined by (55) as function of search point $\hat{y}$ (red solid line) and its theoretical value (56) (blue dashed line). The right picture is a zoom of the left picture.
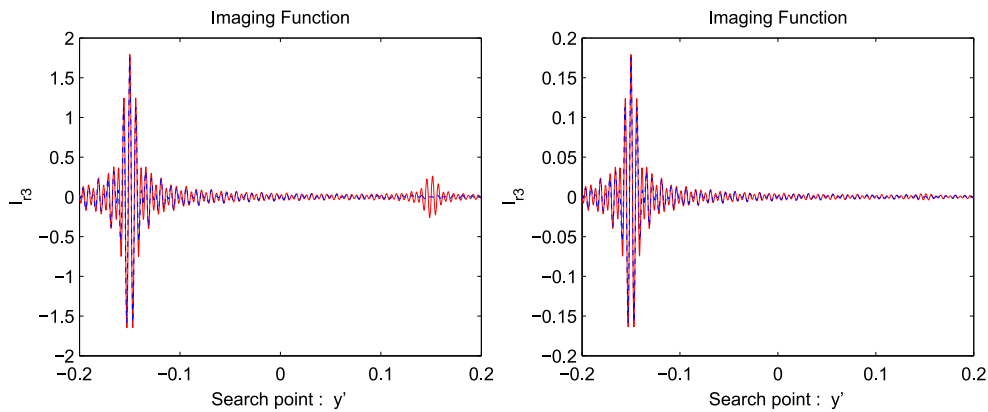


**Figure 8.** The imaging function $\mathcal{I}_{r3}(\hat{y})$ defined by (57) as function of search point $\hat{y}$ (red solid line) and its theoretical value (58) (blue dashed line). In the left picture $D = 10^{-4}$. In the right picture $D = 10^{-5}$.

albeit not completely removed. Indeed we have $n\omega_c D/c_0 \simeq 0.05$, which means that secondary peak is not completely negligible. If we reduce the inclusion width further $D = 10^{-5}$, then $n\omega_c D/c_0 \simeq 0.005$, and the ghost is not visible anymore (its relative amplitude compared to the main peak has been reduced by a factor 10 compared to the case $D = 10^{-4}$), as seen the right picture in figure 8.

### 5.4. Robustness with respect to measurement noise

In the presence of additive noise the measured data have the form

$$a_{\mathrm{mes}}(\omega_m) = \left( a_{3b}(\omega_m) e^{i\omega_m \tau(y_o)} - e^{i\frac{\omega_m}{c_0}(y_o - y_s)} \right) e^{-i\frac{\omega_m}{c_0}(y_o + y_s - L)} + \sigma w_m, \qquad (59)$$

where $w_m$ is an independent and identically distributed sequence of zero mean and unit variance complex circular random variables. The expected value of the imaging function

corresponds to the imaging function in the noise-free case. The variances are

$$
Var\left[\mathcal{I}_{\mathrm{r1}}(\hat{y})\right] = Var\left[\mathcal{I}_{\mathrm{r3}}(\hat{y})\right] = \frac{\omega_c^2 \Delta\omega\sigma^2}{8c_0^2\Omega}\left(1 + \mathcal{R}^4\right).
$$

Therefore the signal-to-noise ratios for the two imaging functions (53) and (57) are

$$
\mathrm{SNR}_1 = \frac{\mathbb{E}\left[\mathcal{I}_{\mathrm{r1}}(y)\right]}{Var\left[\mathcal{I}_{\mathrm{r1}}(\hat{y})\right]^{1/2}} = \frac{\Omega^{1/2}\omega_c D}{c_0\Delta\omega^{1/2}\sigma}\frac{n^2}{4},
$$

$$
\mathrm{SNR}_3 = \frac{\mathbb{E}\left[\mathcal{I}_{\mathrm{r3}}(y)\right]}{Var\left[\mathcal{I}_{\mathrm{r3}}(\hat{y})\right]^{1/2}} = \frac{\Omega^{1/2}\omega_c D}{c_0\Delta\omega^{1/2}\sigma}n,
$$

for large $n$, which confirms that the imaging function (53) is more robust than (57) with respect to measurement noise.

If we assume that the integral in (55) is discretized over the grid $\omega_{\mathrm{m}}$, then we find that

$$
Var\left[\mathcal{I}_{\mathrm{r2}}(\hat{y})\right] = \frac{\omega_c^2\Delta\omega\sigma^2}{2c_0^2\Omega}.
$$

Therefore the signal-to-noise ratio for the imaging function (55) is

$$
\mathrm{SNR}_2 = \frac{\mathbb{E}\left[\mathcal{I}_{\mathrm{r2}}(y)\right]}{Var\left[\mathcal{I}_{\mathrm{r2}}(\hat{y})\right]^{1/2}} = \frac{\Omega^{1/2}\omega_c D}{c_0\Delta\omega^{1/2}\sigma}2\sqrt{2},
$$

for large $n$, which confirms that the imaging function (55) is less robust than (53) and (57) with respect to measurement noise.

### 5.5. Sensitivity with respect to medium uncertainty

As in the source case we assume uncertainty in the medium parameter and examine when this uncertainty leads to a degradation in the image. If the medium parameter $n$ is estimated with an error $\delta$: $1/\hat{n} = (1 + \delta)/n$, then the criterium for the stability of the imaging function (55) is

$$
\delta < \frac{1}{\Omega\tau_L}. \tag{60}
$$

From (55) it is seen that the medium uncertainty gives rise to a shift in the peak (by $\delta L/2$) which will be small compared to the image resolution under the above condition. For the imaging functions (53) and (57) the medium uncertainty translates into a blurring of the peak. Via an analysis as in the case with an internal source we find that this blurring will be relatively small if

$$
\delta < \frac{1}{n\omega_c\tau_L}. \tag{61}
$$

Thus, in conclusion the imaging functions $\mathcal{I}_{\mathrm{r1}}$ and $\mathcal{I}_{\mathrm{r3}}$ are robust with respect to measurement noise, but sensitive with respect to medium uncertainty, while $\mathcal{I}_{\mathrm{r2}}$ is robust with respect to medium uncertainty, but sensitive with respect to measurement noise.

## 6. Conclusions

We have discussed a situation which we believe in a very simple context explains a phenomenon of super resolution as observed in a number of recent studies, including experimental observations [4]. Here the simple mechanism that generates the relatively high resolution is the contrast in wave speed. High resolution or super resolution here refers to resolution better than half the wavelength as recorded by the observer. The main point is indeed that what determines the resolution is the wavelength at the domain of the source or the scatterer to be imaged and not the wavelength as observed in the domain of the recorder. Thus if these have a high contrast we will observe super resolution. Here, we have also analyzed the sensitivity and robustness to measurement noise and medium uncertainty. We find that by exploiting resonance frequencies we can significantly reduce the sensitivity to measurement noise at the expense of relatively high sensitivity to medium uncertainty.

We remark that a similar phenomenon could be observed if the observation point was located in a section of anomalous high velocity, the source could then be localized with far greater accuracy than what is suggested by the wavelength at the point of observation. Indeed, what is important is the velocity contrast in between the source or reflector domain and the domain of observation.

The results presented in this paper have been obtained for the scalar wave equation with a one-dimensional, piecewise constant medium, so as to obtain explicit results that clarify the mechanisms responsible for super-resolution. It is possible to extend the results to continuous media by using the method developed in [12, chapter 4], and to vector waves (such as elastic waves), since the formalism in terms of right- and left-going wave modes is still available in these cases. Generalizations to three-dimensional media by the same technique are not straightforward but they would be possible in some special geometries such as nested radially symmetric or nested hypercube domains.

## Acknowledgements

## Appendix A. The complex amplitude of the recorded field

In the presence of a small inclusion such that

$$n\frac{\omega_c}{c_0}D \ll 1,$$

the expansion of $a_{\mathrm{mes}}(\omega)$ is given by:

$$a_{\mathrm{mes}}(\omega) = \frac{\mathcal{D}_{\mathrm{mes}}(\omega)}{\mathcal{N}_{\mathrm{mes}}(\omega)},$$

$$
\begin{aligned}
\mathcal{D}_{\mathrm{mes}}(\omega) = {}& \mathcal{R}\left( 1 - \mathcal{R}_\alpha^2 \right)\left( \mathrm{e}^{-i\frac{\omega}{c_0}nL} - \mathrm{e}^{i\frac{\omega}{c_0}nL} \right) \\
& + 2i\frac{\omega}{c_0}D\frac{\mathcal{R}_\alpha}{\alpha}\left( \mathrm{e}^{-2i\frac{\omega}{c_0}ny} + \mathcal{R}^2 \mathrm{e}^{2i\frac{\omega}{c_0}ny} \right) \\
& + i\frac{\omega}{c_0}D\mathcal{R}\left( n\left( 1 - \mathcal{R}_\alpha^2 \right) - \frac{1}{\alpha}\left( 1 + \mathcal{R}_\alpha^2 \right) \right)\left( \mathrm{e}^{-i\frac{\omega}{c_0}nL} + \mathrm{e}^{i\frac{\omega}{c_0}nL} \right) \\
& + O\left( n^2 \frac{\omega^2}{c_0^2}D^2 \right),
\end{aligned}
$$

$$
\begin{aligned}
\mathcal{N}_{\mathrm{mes}}(\omega) = {}& \left( 1 - \mathcal{R}_\alpha^2 \right)\left( \mathrm{e}^{-i\frac{\omega}{c_0}nL} - \mathcal{R}^2 \mathrm{e}^{i\frac{\omega}{c_0}nL} \right) \\
& + 2i\frac{\omega}{c_0}D\frac{\mathcal{R}\mathcal{R}_\alpha}{\alpha}\left( \mathrm{e}^{-2i\frac{\omega}{c_0}ny} + \mathrm{e}^{2i\frac{\omega}{c_0}ny} \right) \\
& + i\frac{\omega}{c_0}D\left( n\left( 1 - \mathcal{R}_\alpha^2 \right) - \frac{1}{\alpha}\left( 1 + \mathcal{R}_\alpha^2 \right) \right)\left( \mathrm{e}^{-i\frac{\omega}{c_0}nL} + \mathcal{R}^2 \mathrm{e}^{i\frac{\omega}{c_0}nL} \right) \\
& + O\left( n^2 \frac{\omega^2}{c_0^2}D^2 \right).
\end{aligned}
$$

# References

[1] Ammari H, Bonnetier E and Capdeboscq Y 2009 Enhanced resolution in structured media *SIAM J. Appl. Math.* **70** 1428–52

[2] Ammari H, Garnier J, Kang H, Park W K and Sølna K 2011 Imaging schemes for perfectly conducting cracks *SIAM J. Appl. Math.* **71** 68–91

[3] Ammari H, Garnier J, Jing W, Kang H, Lim M, Sølna K and Wang H 2013 *Mathematical and Statistical Methods for Multistatic Imaging (Lecture Notes in Mathematics vol 2098)* (Berlin: Springer)

[4] Arhab S, Soriano G, Maire G, Talneau A, Sentenac D, Chaumet P C, Belkebir K and Giovannini H 2013 Nanometric resolution with far-field optical profilometry *Phys. Rev. Lett.* **111** 053902

[5] Baggeroer A B, Kuperman W A and Schmidt H 1988 Matched field processing: source localization in correlated noise as an optimum parameter estimation problem *J. Acoust. Soc. Am.* **83** 571–87

Baggeroer A B, Kuperman W A and Mikhalevsky P N 1993 An overview of matched field methods in ocean acoustics *IEEE J. Ocean. Eng.* **18** 401–24

[6] Borcea L, Papanicolaou G, Tsogka C and Berryman J 2002 Imaging and time reversal in random media *Inverse Problems* **18** 1247–79

[7] de Rosny J and Fink M 2002 Overcoming the diffraction limit in wave physics using a time-reversal mirror and a novel acoustic sink *Phys. Rev. Lett.* **89** 124301

[8] de Rosny J and Fink M 2007 Focusing properties of near-field time reversal *Phys. Rev. A* **76** 065801

[9] Fink M 1992 Time reversal of ultrasonic fields. I. Basic principles *IEEE Trans. Ultrason. Ferroelectr. Frequation Control* **39** 555–66

[10] Fink M 1999 Time reversed acoustics *Sci. Am.* **281** 91–7

[11] Fink M, Cassereau D, Derode A, Prada C, Roux P, Tanter M, Thomas J-L and Wu F 2000 Time-reversed acoustics *Rep. Prog. Phys.* **63** 1933–95

[12] Fouque J-P, Garnier J, Papanicolaou G and Sølna K 2007 *Wave Propagation and Time Reversal in Randomly Layered Media* (New York: Springer)

[13] Gomez C 2009 Time-reversal superresolution in random waveguides *SIAM Multiscale Model. Simul.* **7** 1348–86

[14] Guckenheimer J and Holmes P J 1983 *Nonlinear Oscillations, Dynamical Systems, and Bifurcations of Vector Fields* (New York: Springer)

[15] Lemoult F, Fink M and Lerosey G 2012 A polychromatic approach to far-field superlensing at visible wavelengths *Nat. Commun.* **3** 889

[16] Lemoult F, Fink M and Lerosey G 2011 Acoustic resonators for far-field control of sound on a subwavelength scale *Phys. Rev. Lett.* **107** 064301

[17] Lemoult F, Ourir A, de Rosny J, Tourin A, Fink M and Lerosey G 2010 Resonant metalenses for breaking the diffraction barrier *Phys. Rev. Lett.* **104** 203901

[18] Lerosey G, de Rosny J, Tourin A and Fink M 2007 Focusing beyond the diffraction limit with far-field time reversal *Science* **315** 1120–2

[19] Ourir A, Lerosey G, Lemoult F, Fink M and de Rosny J 2012 Far field subwavelength imaging of magnetic patterns *Appl. Phys. Lett.* **101** 111102

[20] Soares C and Jesus S M 2003 Broadband matched-field processing: coherent and incoherent approaches *J. Acoust. Soc. Am.* **113** 2587–98